Response of Atmospheric Convection to Vertical Wind Shear: Cloud Resolving Simulations with Parameterized Large-Scale Circulation.

Part II: Effect of Interactive Radiation

Usama Anber[1,3], Shuguang Wang[2], and Adam Sobel [1,2,3]

1 Lamont-Doherty Earth Observatory of Columbia University, Palisades, NY

2 Department of Applied Physics and Applied Mathematics, Columbia University, New York, NY

3 Department of Earth and Environmental Sciences, Columbia University, New York, NY

Corresponding Author: Usama Anber, Lamont-Doherty Earth Observatory, 61 Route 9W, Palisades, NY 10964. E-mail: uanber@ldeo.columbia.edu

ABSTRACT

The authors investigate the effects of cloud-radiation interaction and vertical wind shear on convective ensembles interacting with large scale dynamics in cloud resolving model simulations, with the large-scale circulation parameterized using the weak temperature gradient approximation. Numerical experiments with interactive radiation are conducted with imposed surface heat fluxes constant in space and time, an idealized lower boundary condition which prevents wind-evaporation feedback. Each simulation with interactive radiation is compared to a simulation in which the radiative heating profile is held constant in the horizontal and time, and is equal to the horizontal mean profile from the interactive radiation simulation with the same vertical shear and surface fluxes. Interactive radiation is found to reduce mean precipitation in all cases. The magnitude of the reduction is nearly independent of the vertical wind shear, but increases with surface fluxes. Deep shear also reduces precipitation, though by approximately the same amount with or without interactive radiation. The reductions in precipitation due to either interactive radiation or deep shear are associated with large-scale descent in the lower troposphere, which more strongly exports moist static energy and is quantified by a larger normalized gross moist stability.

1. Introduction

Radiative feedbacks have been shown to contribute to the dynamics of tropical disturbances on a range of time scales. The phenomena influenced by these feedbacks include tropical cyclogenesis (e.g. Bu et al 2014; Hakim 2013) and intraseasonal variability (e.g., Raymond 2001; Bony and Emanuel 2005; Kim et al. 2011; Sobel and Maloney 2013), and have been found in observations (e.g. Lin and Mapes 2004; Sobel et al. 2014) as well as idealized numerical modeling studies (e.g., Raymond 2001; Grabowski and Moncrieff 2002; Bony and Emanuel 2005; Wing and Emanuel 2014).

By absorbing longwave radiation and re-emitting it to space at lower temperatures, clouds and water vapor warm the troposphere. Locally, regions of deep convection experience a strong reduction in the net radiative cooling compared to adjacent clear-sky regions. At the top of the atmosphere, this longwave warming is often largely (though imperfectly; Lin and Mapes 2004), offset by shortwave anomalies due to the enhanced albedo of deep clouds (e.g., Ramanathan et al. 1989; Hartmann et al. 2001), so that the effect of high tropical clouds on the long-term climate is modest. However, the longwave effect is felt immediately in the atmosphere, while the compensating shortwave effect is felt largely at the surface. If the surface is ocean, the heat capacity of the ocean mixed layer can delay the surface response enough that on short time scales, the positive feedback in the atmosphere dominates. By acting as a source of column-integrated moist static energy where that quantity already has a positive anomaly, this longwave radiative feedback is positive, and can organize tropical convection on a range of scales, including the intraseasonal (Raymond 2001; Sobel and Gildor 2003; Grabowski and Moncrieff

2004; Bretherton et al. 2005; Wing and Emanuel 2014; Emanuel et al. 2014; Tobin et al. 2013; Chikira 2014).

We expect the effectiveness of cloud-radiative feedbacks to be related to the horizontal extent, vertical structure and microphysical properties of the cloud field. These cloud properties, in turn, are influenced by a number of environmental factors. Vertical wind shear is an important such factor, in that we expect it to play a significant role in the organization of convective cloud systems on the mesoscale. In this study, we describe studies designed to isolate the effects of interactive radiation and vertical shear, together and separately, on tropical oceanic convection.

In the first part of this study (Anber et al. 2014 hereafter AWS14), we performed CRM simulations in which we prescribed both surface fluxes and column radiative heating, and introduced a background vertical wind shear of different strengths as a control parameter. We found that under otherwise identical large-scale conditions, the precipitation can change significantly as a result of the wind shear influence, as the shear organizes the convective systems into squall line-like structures. These structures influence the convective heating and large-scale vertical motion profiles, with the relationship between heating and large-scale vertical motion parameterized in AWS14 by the weak temperature gradient (WTG) approximation. The different vertical motion profiles lead to different mean precipitation rates for the same export of moist static energy (with that export fixed in the experiments of AWS14 by the imposed surface fluxes and radiative cooling), a relationship quantified by the normalized gross moist stability.

In this sequel paper we perform similar model integrations, again studying the influence of vertical wind shear on tropical convection, but now with interactive radiative heating. The results are then compared to those obtained from otherwise identical experiments in which the radiative heating is prescribed to have the same profile in the time mean as the interactive radiation simulations.

Our simulation design is such that we are not studying the most direct aspects of the radiative feedback on convective organization, in which the radiative heating itself changes on the large scale (represented in our simulations by the horizontal and time mean over the domain). We compare interactive- and fixed-radiation simulations in which the radiative heating itself is the same in the horizontal and time mean. The direct radiative feedback relevant to tropical disturbances can be estimated straightforwardly, from observations or global model simulations, as the column-integrated radiative heating anomaly per unit anomaly in column water vapor, precipitation, or other metric of convective activity on the space and time scale of interest (e.g., Bretherton and Sobel 2002; Su and Neelin 2002; Lin and Mapes 2004). Rather, we investigate the more indirect effects which result not from the change in the areally averaged radiative heating, but from the effects that *interactive* radiation may have on cloud structure and dynamics, holding the large-scale mean radiative heating profile fixed. These interactivity effects then change the cloud system structure and horizontal mean latent heating, and influence the export of moist static energy via changes in the large-scale vertical motion profile associated with those latent heating changes. We find that these effects can be quite significant. We are not aware of any previous documentation of them.

To facilitate our focus on the vertical shear influence and cloud-radiative interaction, we prescribe surface turbulent heat fluxes. This eliminates surface flux feedbacks which would occur if the lower boundary were taken to be at fixed sea surface temperature (SST). With varying vertical shear, changes in momentum transport to the surface can change surface winds from one simulation to the next, inducing strong surface turbulent flux feedbacks under fixed SST. These feedbacks are not of interest here, so we eliminate them by prescribing surface turbulent heat fluxes directly. We have also conducted simulations with a slab ocean model; these increase the size of the parameter space and the range of possible model behavior enough that we will report on them in a separate study.

After describing the model and experiment design in section 2, we present the results in section 3. We summarize in section 4.

2. Model and Experiment Design

The model used here is the Weather Research and Forecast (WRF) model version 3.3, in three spatial dimensions with the same physical parameterization schemes used in AWS14. For experimental design and implementation of the weak temperature gradient (WTG) approximation (Sobel and Bretherton 2000; Raymond and Zeng 2005) the reader is referred to AWS14. All experiments are integrated more than 40 days to achieve statistical equilibrium, and analysis of the output is conducted on the last 20 days, during which the simulations have reached statistical equilibrium.

To obtain the reference temperature profile required for WTG, we follow a standard procedure (e.g., Sobel and Bretherton 2000; Raymond and Zeng 2005; Wang

and Sobel 2011; Daleu et al. 2015). We first perform a radiative-convective equilibrium (RCE) experiment at a fixed SST of 28 ℃ with interactive radiation, reaching equilibrium at about 60 days. Results from this experiment are averaged over the last 10 days after equilibrium to obtain statistically equilibrated temperature and moisture profiles. Figure 1 shows the resulting vertical profiles of (a) potential temperature and (b) moisture. These profiles are then used to initialize runs with parameterized large scale circulation, and the temperature profile is used as the target profile against which perturbations are computed in the WTG runs.

For our experiments with interactive radiation, the NCAR Community Atmosphere Model (CAM 3.0) shortwave and longwave radiation schemes (Collins et al. 2004) are used. Diurnal and seasonal cycles are removed and the top of the atmosphere incident solar flux is set to 400 W m^{-2}.

For WTG runs without vertical wind shear, we prescribe total turbulent surface fluxes of heat and moisture at three different values: low (140 W m^{-2}), moderate (180 W m^{-2}), and high (220 W m^{-2}); these variations are achieved holding the sensible heat flux fixed at 20 W m^{-2} while the latent heat flux takes on values of 120, 160, and 200 W m^{-2}, respectively.

We constrain the vertical wind shear by relaxing the horizontal mean zonal wind towards a prescribed profile with a time scale of one hour, as in AWS14. We vary the shear depth over three layers; shallow (1500 m), midlevel (4500 m), and deep (12000 m), while holding the target wind speed at the top of the shear layer constant at 20 m/s, and keeping it zero at the surface (see Fig.1 of AWS14). Surface fluxes for this set of experiments are held fixed at 140, 180, and 220 W m^{-2} but we show results from the case

of 180 W m^{-2} only since results from other cases are similar and same conclusion can be made. Clouds and water vapor then evolve freely and strongly influence the radiative heating profile.

The time-and domain-averaged radiative heating profiles for this set of experiments is shown in Fig. 2*a* for the unsheared environment with different surface fluxes, and Fig. 2*b* for different shear depths with intermediate surface fluxes. For either low surface fluxes or shallow shear there is a cooling throughout the whole atmospheric column that reaches 1 K/day in the upper troposphere. For higher surface fluxes or deeper shear, there is a significant radiative heating in the mid-to upper troposphere, exceeding 5 K/day for high surface fluxes. Above 10 Km there is a sharp drop in the radiative heating profile due to the strong emission of longwave radiation from cloud top, with radiative cooling exceeding 10 K/day for strong surface fluxes or deep shear.

To compare the effect of interactive radiation on the cumulus ensemble interacting with the parameterized large scale dynamics, we perform a set of experiments identical to those described above except that we prescribe the radiative cooling profile in Figure 2 and keep it constant in both the horizontal and time. This the time-and domain-averaged radiative cooling is the same with either fixed or interactive radiation. As surface fluxes are already fixed, this means that both the equilibrated time mean column-integrated moist static surface fluxes and net radiative cooling are identical in pairs of interactive- and fixed-radiation experiments. Any differences in the time mean column moist static energy budgets must be due to the export term, which is controlled by the large-scale vertical velocity profile.

3. Results

Fig.3 shows time and domain averaged precipitation, *P,* as a function of (a) surface fluxes in unsheared environment and (b) wind shear at moderate surface fluxes of 180 W m^{-2} (shear cases at low and high surface fluxes are similar and not shown), for experiments with interactive radiation (blue) and prescribed radiation (red). In all pairs of experiments, interactive radiation produces significantly less precipitation than does prescribed radiation. The difference monotonically increases with surface fluxes (Fig. 3a). The difference is about 1mm/d for small surface fluxes, and reaches 3 mm/d and 5 mm/d for the moderate and high surface fluxes, respectively, while remaining nearly constant with shear (Fig. 3b). Mid-level shear produces the greatest precipitation in both interactive as well as prescribed radiation experiments. A non-monotonic relation between shear and precipitation was also found in the first part of this study, with specified radiative cooling, and in other studies with different methodologies (e.g. AWS14, Weisman et al. 2004).

Precipitation is also diagnosed from the combined vertically integrated budgets of moist and dry static energy as:

$$P = \frac{1}{M}(L + H + \langle Q_R \rangle) - \langle Q_R \rangle - H$$

where *L,H,* $< Q_R >$, and *M* are the latent heat flux, sensible heat flux, vertically integrated radiative heating, and normalized gross moist stability, respectively. The latter is defined as $M = \left\langle \overline{W}\frac{\overline{\partial h}}{\partial z} \right\rangle \Big/ \left\langle \overline{W}\frac{\overline{\partial s}}{\partial z} \right\rangle$

where *W*, *s,* and *h* are the large-scale vertical velocity, dry, and moist static energy (MSE) respectively, brackets denote mass weighted vertical integrals, and overbars are domain

177 and time mean. The above equation gives very good agreement with the model output as
178 indicated in Fig.3 with square symbols. The above equation helps us to interpret changes
179 in *P*.

180 To understand the behavior of precipitation in the presence of cloud-radiation
181 interaction, we look at the large-scale vertical motion W_{WTG}. Figure 4 shows the vertical
182 profile of W_{WTG} with surface fluxes of 140, 180, and 220 W m^{-2} ((a), (b), and (c),
183 respectively), in the unsheared environment, and shear depths of 1500 m, 4500 m, and
184 12000 m ((d), (e), and (f), respectively), with intermediate surface fluxes, for both
185 interactive (solid curves) and prescribed (dashed) radiative cooling. In all cases, when
186 radiation is interactive the large scale vertical motion exhibits a qualitatively similar
187 vertical structure to that when radiation is prescribed, but with a sharper peak at about 10
188 km and stronger subsidence in the lower levels (except in the shallow shear case, Fig.
189 4d), especially for the high surface flux and deep shear cases.

190 A closer look at the peak magnitude of the ascent and descent is shown in Fig. 5,
191 which displays the maximum and minimum values of the W_{WTG} profile as a function of
192 surface fluxes and shear depth. The peak amplitude of the vertical motion is a
193 monotonically increasing function of the surface fluxes and the shear depth for both
194 interactive and prescribed radiative heating. However, there are significant differences
195 between the two mean profiles. Except for the shallow shear depth where the heating
196 anomalies are negative, such heating anomalies increase with either increasing surface
197 fluxes or shear depth, and reach maximum amplitude for the highest surface fluxes and
198 largest shear depth.
199

The most striking feature in the large scale vertical velocity structure is the significant subsidence in the lower troposphere, resulting from evaporative cooling under mesoscale cloud systems. For low and moderate surface fluxes, interactive radiation introduces a small increase in this subsidence, and for shallow and midlevel shear the difference in subsidence introduced by interactive radiation is small. However, for the high surface fluxes and deep shear cases, interactive radiation strongly strengthens this lower-tropospheric subsidence. This is particularly important in the moist static energy budget.

This indirect role of interactive radiation in the thermodynamics can be usefully interpreted in terms of the normalized gross moist stability (e.g. Neelin and Held 1987; Sobel 2007) shown in Figure 6, and defined above as the export of moist static energy normalized by the export of dry static energy. Increasing surface fluxes while holding the radiative heating prescribed does not have a strong impact on M. For interactive radiation, however, as the surface fluxes increase, M increases strongly. Introduction of deep shear also increases M, but does so similarly whether radiation is fixed or interactive. These increases are results of stronger ascent in the upper troposphere and descent in the lower troposphere, implying horizontal divergence both at upper levels and near the surface where moist static energy is large, and convergence in mid-troposphere where it is smaller. M exceeds unity for the greatest surface fluxes and shear depth, meaning that the export of moist static energy exceeds the export of dry static energy, as seen late in the active phases of the MJO (e.g. Wang et al. 2015; Sobel et al. 2014). Any increase in radiative heating or surface fluxes for $M > 1$ is relatively inefficient in

223 increasing precipitation since P is inversely proportional to the product of $1/M$ and these
224 MSE sources.

225 The strong increase in M in the interactive vs. fixed radiation experiments was
226 unexpected, and implies some cancellation between direct and indirect effects of
227 radiation in the moist static energy budgets of deep convective tropical disturbances. In
228 our simulations, the direct radiative feedback (defined operationally here as the horizontal
229 mean radiative cooling change as a function of precipitation or other measure of
230 convective activity) is present only implicitly, since interactive- and fixed-radiation
231 experiments with the same surface fluxes share the same time-mean radiative heating
232 profiles. We expect this direct feedback to be positive, reducing the radiative cooling in
233 the presence of large high cloud cover and column humidity and thus providing an
234 anomalous source of MSE to the column. Our results imply that the radiative feedback
235 also has a significant indirect effect which opposes this, changing the large-scale vertical
236 motion profile so as to drive stronger advective export of MSE, thus acting as an
237 anomalous sink of that quantity.

238 This result may be relevant to a number of observed phenomena; one that occurs to us in
239 particular is the MJO. As shown in several studies (e.g., Yasunaga and Mapes 2012; Kim
240 et al. 2014; Sobel et al. 2014; Inoue and back 2015a, 2015b), the maximum in
241 precipitation associated with the MJO active phase occurs nearly simultaneously with the
242 maximum in column-integrated MSE over the Indian Ocean. Column-integrated vertical
243 advection of MSE is negative (i.e., export; positive M) during the active phase, and
244 increases in magnitude as the phase advances, with minimum M before the peak MSE
245 and precipitation and maximum after it (in either longitude or time). These variations in

246 vertical advection are associated with the MJO's eastward propagation, as anomalous
247 MSE import ahead acts to increase MSE leading up to the peak in the active phase, and
248 anomalous export afterwards acts to reduce it (e.g., Kiranmayi and Maloney 2011; Kim et
249 al. 2014; Sobel et al 2014; Inoue and Back 2015a, b; Yokoi and Sobel 2015).

250 The progression in the vertical motion profile to greater top-heaviness as the
251 MJO's active phase matures is associated with a gradual transition from more convective
252 to more stratiform cloud types, similar to what happens in individual mesoscale systems,
253 but on much larger scales in both space and time (Mapes 2006). While the dynamics of
254 the convective-stratiform transition are understood on the mesoscale, it has been unclear
255 what mechanisms cause such a similar transition to play out on the planetary scale of the
256 MJO, where it is not associated with individual mesoscale convective systems but rather
257 a much larger envelope containing many such systems. While by no means solving this
258 puzzle completely, our results suggest that both vertical shear and cloud-radiative
259 interactions – both of which are strong in the late active phase of the MJO - may play key
260 roles on this larger scale.

261

262 Finally, the temperature anomalies associated with interactive radiation are
263 relevant to understanding the changes in vertical motion described above. Figure 7 shows
264 the mean temperature anomalies from the RCE temperature profile as a function of
265 surface fluxes (a), and shear depths (b). The low surface flux and shallow shear cases
266 show warm anomalies throughout the atmosphere. However, as the surface fluxes or
267 shear depth increase, the warm anomalies in the upper troposphere, and cool anomalies in
268 the lower troposphere both strengthen. These temperature anomaly profiles indicate a

more stable environment, as usually observed in mesoscale convective systems and associated with horizontally extensive stratiform cloud and a second baroclinic mode component to the heating profile (Houze 1989).

5. Summary

We have presented results from idealized 3D cloud resolving simulations with large-scale circulation parameterized under the weak temperature gradient approximation to investigate the effects of interactive radiation and vertical shear on tropical deep convection. Surface fluxes of heat and moisture were prescribed to remove wind-surface flux feedbacks, and results were presented for different imposed vertical wind shear profiles as well as different surface flux magnitudes. Results from simulations with fixed and interactive radiation were compared, with the two types of simulations having the same time-mean radiative heating profile so that any difference is only due to the interactivity itself. The direct radiative-convective feedback, associated with changes in the domain-averaged radiative heating profile (e.g., as a function of precipitation or column water vapor) was excluded.

Interactive radiation has a significant impact when high surface fluxes are high, by generating a stronger envelope of high anvil cloud that extends over a large horizontal extent. The heating profile associated with this cloud system, via WTG, strengthens large-scale ascent in the upper troposphere and causes descent in the lower troposphere. This results in an increase in the normalized gross moist stability, and a decrease in mean precipitation, as moist static energy is more efficiently exported by the more top-heavy ascent profile. Deep vertical shear has a similar effect; it has this effect with either fixed

or interactive radiation, but the reduction in precipitation due to strong moist static energy is greatest when both deep shear and interactive radiation are present. We suggest that this behavior is relevant to the late active phase of the Madden-Julian oscillation (MJO), in which deep, strong vertical shear is present and surface fluxes are large. Coupling between radiation and dynamics of the type simulated here may be relevant to the increase in normalized gross moist stability which is found in observations late in the active phase of the MJO (Kim et al. 2014; Sobel et al. 2014; Inoue and Back 2015a,b), and which plays a significant role in the MJO's eastward propagation.

Acknowledgement

This work was supported by NSF grant AGS-1008847. We acknowledge high-performance computing support from Yellowstone (ark:/85065/d7wd3xhc) provided by NCAR's Computational and Information Systems Laboratory, sponsored by the National Science Foundation.

References

Anber, S., Wang, and A. H., Sobel, 2014: Response of atmospheric convection to vertical wind shear: cloud resolving simulations with parameterized large-scale circulation. Part I: Specified radiative cooling. *J. Atmos. Sci.*

Anber, S., Wang, and A. H., Sobel, 2015: Effect of surface fluxes versus radiative heating on tropical deep convection. *Under review*

Bister, M., and K.A. Emanuel, 1997: The genesis of Hurricane Guillermo: TEXMEX analyses and a modeling study. *Mon. Wea. Rev*., **125**, 2662-2682.

Bony, S., and K. A. Emanuel, 2005: On the role of moist processes in tropical

Intraseasonal variability: cloud–radiation and moisture–convection Feedbacks. *J. Atmos. Sci.*, **62**, 2770–2789.

Bretherton, C. S., P. N. Blossey, and M. Khairoutdinov, 2005: An energy-balance analysis of deep convective self-aggregation above uniform SST. *J. Atmos. Sci.*, **62**, 4273–4292.

Bu Y., Robert G. Fovell, and Kristen L. Corbosiero, 2014: Influence of Cloud–Radiative Forcing on Tropical Cyclone Structure. *J. Atmos. Sci.*, **71**, 1644–1662.

Chikira, M., 2014: Eastward-propagating intraseasonal oscillation represented by Chikira–Sugiyama cumulus parameterization. Part II: Understanding moisture variation under weak Temperature gradient balance. *J. Atmos. Sci.,* **71**, 615-639.

Collins, W. D., et al. (2004), Description of the NCAR Community Atmosphere Model: CAM3.0, *Tech. Rep. NCAR/TN-464+STR*, 226 pp.

Daleu, C. L., S. J. Woolnough, R. S. Plant, S. Sessions, M. J. Herman, A. Sobel, S. Wang, D. Kim, A. Cheng, G. Bellon, P. Peyrille, F. Ferry, A. P. Siebesma, and B. van Ulft, 2015: Intercomparison of methods of coupling between convection and large-scale circulation. Part I: Comparison over uniform surface conditions. *J. Adv. Model. Earth Sys.,* submitted.

355 Emanuel, K., A. A. Wing, and E. M. Vincent, 2014: Radiative-Convective Instability. *J.*
356 *Adv. Model. Earth Sys*., **6**, doi:10.1002/2013MS000270.
357
358 Fu, Q., and K. N. Liou, 1993: Parameterization of the radiative properties of cirrus
359 clouds. J. Atmos. Sci., 50, 2008-2025
360
361 Grabowski, W. W., and M. W. Moncrieff, 2001: Large-scale organization of tropical
362 convection in two-dimensional explicit numerical simulations: Effects of interactive
363 radiation. Quart. J. Roy. Meteor. Soc., 128, 2349–2375.
364
365 Hakim, G. J., 2013: The variability and predictability of axisymmetric hurricanes in
366 statistical equilibrium. *J. Atmos. Sci.*, **70,** 993-1005.
367
368 Hartmann, Dennis L., Leslie A. Moy, Qiang Fu, 2001: Tropical Convection and the
369 Energy Balance at the Top of the Atmosphere. *J. Climate*, **14**, 4495–4511.
370
371 Houze, R. A., Jr., 1989: Observed structure of mesoscale convective systems and
372 implications for large-scale heating. Quart. J. Roy. Meteor. Soc., 115, 425–461.
373
374 Inoue, K. and L.E. Back, 2015a: Gross moist stability assessment during TOGA COARE:
375 Various interpretations of gross moist stability. Submitted to J. Atmos. Sci.
376

377 Inoue, K. and L.E. Back, 2015b: Column-Integrated Moist Static Energy Analysis on
378 Various Time Scales during TOGA COARE. Accepted by J. Atmos. Sci.
379
380 Johnson, R. H., and P. E. Ciesielski, 2000: Rainfall and radiative heating rates from
381 TOGA COARE atmospheric budgets. J. Atmos. Sci., 57, 1497–1514.
382
383 Kim, D., A. H. Sobel, and I.-S. Kang, 2011: A mechanism denial study on the Madden-
384 Julian oscillation. *J. Adv. Model. Earth Sys.,***3**, M12007.
385
386 Kim, D., J.-S. Kug, and A. H. Sobel, 2014: Propagating vs. Non-propagating Madden-
387 Julian oscillation events. *J. Climate*, **27**, 111-125.
388
389 Kiranmayi, L., and E. D. Maloney, 2011: Intraseasonal moist static energy budget in
390 reanalysis data. *J. Geophys. Res.***, 116**, DOI**:** 10.1029/2011JD016031
391
392 Lin, Jia-Lin, Brian E. Mapes, 2004: Radiation Budget of the Tropical Intraseasonal
393 Oscillation. *J. Atmos. Sci.*, **61**, 2050–2062.
394
395 Mapes, B., S. Tulich, J. Lin, and P. Zuidema, 2006: The mesoscale convection life cycle:
396 Building block or prototype for large-scale tropical waves? *Dyn. Atm. Oceans,* **42**, 3-29.
397
398 Neelin, J. D., and I. M. Held (1987), Modeling tropical convergence based on the moist
399 static energy budget, *Mon. Wea. Rev.*, **115**, 3–12, doi:10.1175/1520-

0493(1987)115<0003:MTCBOT>2.0.CO;2

Ramanathan, V., R. D. Cess, E. F. Harrison, P. Minnis, B. R. Barkstrom, E. Ahmad, and D. Hartmann, 1989: Cloud-radiative forcing and climate: Results from the Earth Radiation Budget Experiment. *Science,* **243**, 57-63.

Raymond, D. J., 2001: A new model of the Madden–Julian oscillation. J. Atmos. Sci., 58, 2807–2819.

Raymond, D. J., and S. L. Sessions, 2007: Evolution of convection during tropical cyclogenesis, Geophys. Res. Lett., 34, L06811, doi:10.1029/2006GL028607.

Raymond, D. J., and X. Zeng, 2000: Instability and large-scale circulations in a two-column model of the tropical troposphere, Quart. J. Roy. Meteor. Soc., 126, 3117-3135

Raymond, D. J., and X. Zeng, 2005, Modelling tropical atmospheric convection in the context of the weak temperature gradient approximation, *Q. J. R. Meteorol. Soc.,* 131, 1301–1320.

Sobel, A. H. (2007), Simple models of ensemble-averaged tropical precipitation and surface wind, *The Global Circulation of the Atmosphere*, Princeton University Press, T. Schneider, and A. H. Sobel.

Sobel, A. H., and C. S. Bretherton, 2000, Modeling tropical precipitation in a single column, *J. Clim.*, 13, 4378–4392.

Sobel, A. H., and E. D. Maloney, 2013: Moisture modes and the eastward propagation of the MJO. *J. Atmos. Sci.,* **70**, 187-192.

Sobel, A. H., E. D.Maloney, G.Bellon, and D. M.Frierson (2008), The role surface heat fluxes in tropical intraseasonal oscillations, *Nat. Geosci.*, **1**, 653–657.

Sobel, A. H., E. D.Maloney, G.Bellon, and D. M.Frierson (2010), Surface fluxes and tropical intraseasonal variability: A reassessment, *J. Adv. Model. Earth Syst.*, **2**, 2.

Sobel, A., Wang, S., and Kim, D., 2014: Moist static energy budget of the MJO during DYNAMO. *Journal of the Atmospheric Sciences*, **71**, 4276-4291.

Su, H., and J. D. Neelin 2002: Teleconnection mechanisms for tropical Pacific descent anomalies during El Nino. *J. Atmos. Sci.,* **59**, 2694-2712.

Tobin, I., Sandrine Bony, Chris E. Holloway, Jean-Yves Grandpeix, Geneviève Sèze, David Coppin, Steve J. Woolnough, Rémy Roca. (2013) Does convective aggregation need to be represented in cumulus parameterizations?. *Journal of Advances in Modeling Earth Systems* **5**:10.1002/jame.v5.4, 692-703.

446 Wang, S., A. H. Sobel, and Z. Kuang, 2013: Cloud-resolving simulation of TOGA-
447 COARE using parameterized large-scale dynamics. *J. Geophys. Res.*, 118,
448 doi:10.1002/jgrd.50510.
449
450 Wang, S., A. H. Sobel, F. Zhang, Y. Q. Sun, Y. Yue, and L. Zhou, 2015: Regional
451 simulation of the October and November MJO events observed during the
452 CINDY/DYNAMO field campaign at gray zone resolution. *Journal of Climate*, **28**, 2097-
453 2119.
454
455 Weisman, M. L., and R. Rotunno, 2004: "A Theory for Strong Long-Lived Squall Lines"
456 Revisited. *J. Atmos. Sci.*, **61**, 361–382.
457
458 Wing, A. A., and K. A. Emanuel, 2014: Physical mechanisms controlling self-
459 aggregation of convection in idealized numerical modeling simulations. *J. Adv. Model.*
460 *Earth Sys*., **6**, doi:10.1002/2013MS000269.
461
462 Woolnough, S. J., J. M. Slingo, and B. J. Hoskins (2000), The relationship between
463 convection and sea surface temperature on intraseasonal timescales, J. Climate, 13, 2086–
464 2104.
465
466 Yasunaga, K., and B. E. Mapes, 2012: Differences between more divergent vs. more-
467 rotational types of convectively coupled equatorial waves. Part I: Space–time spectral
468 analyses. *J. Atmos. Sci.,* **69**, 3–16, doi:10.1175/JAS-D-11-033.1.

List of Figures

FIG.7. Domain mean profile of temperature anomalies, as departure from RCE profile, as a function of (a) surface fluxes, and (b) vertical shear depths.

Figures

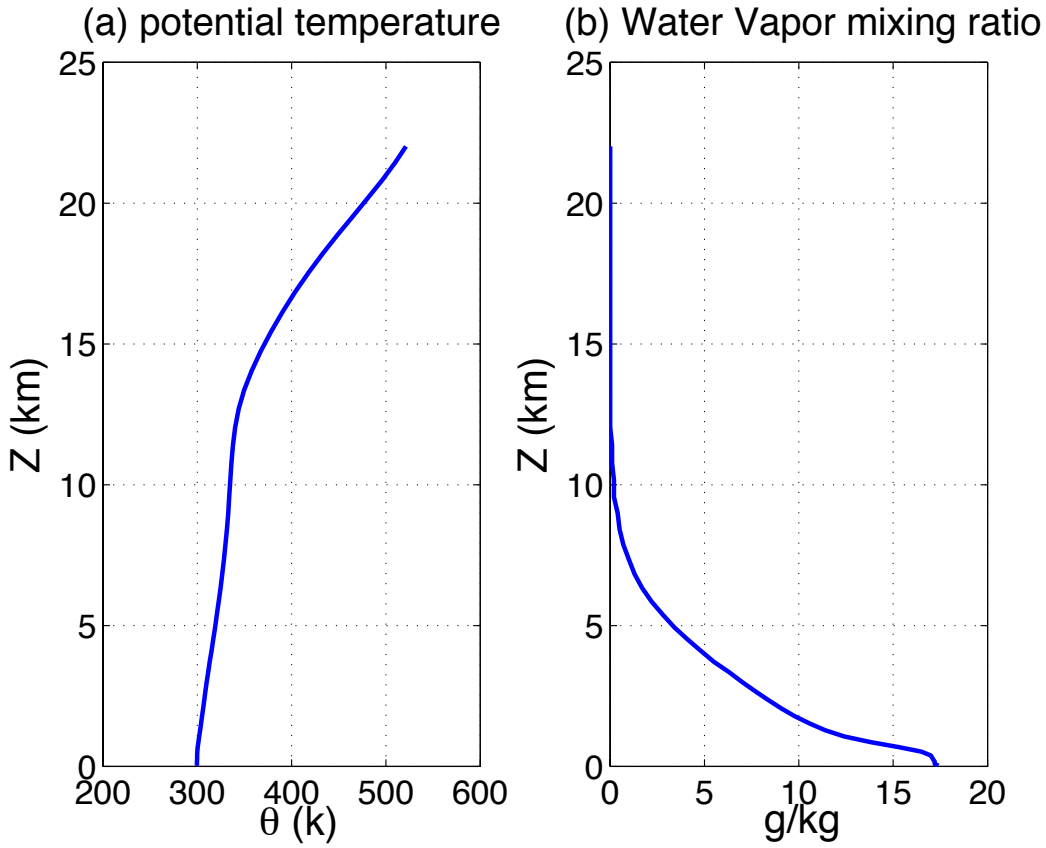

FIG.1. Equilibrium vertical profiles of (a) potential temperature and (b) water vapor mixing ratio from the RCE simulation.

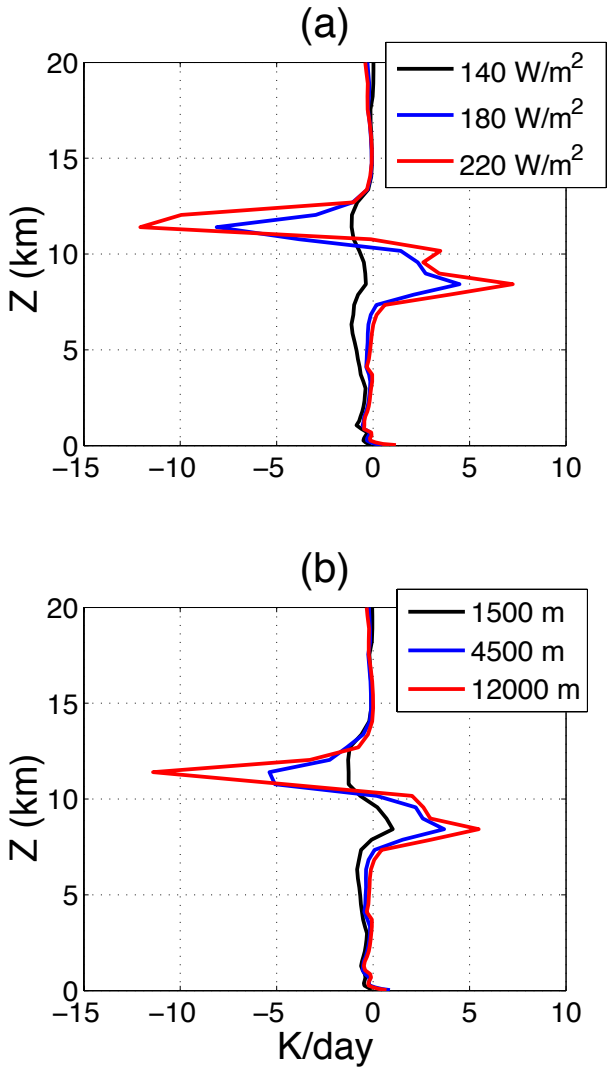

524

525 FIG.2. Domain averaged radiative cooling profile as a function of (a) surface fluxes in

526 unsheared environment, and (b) shear depths at surface fluxes of 180 W m^{-2}.

527

528

529

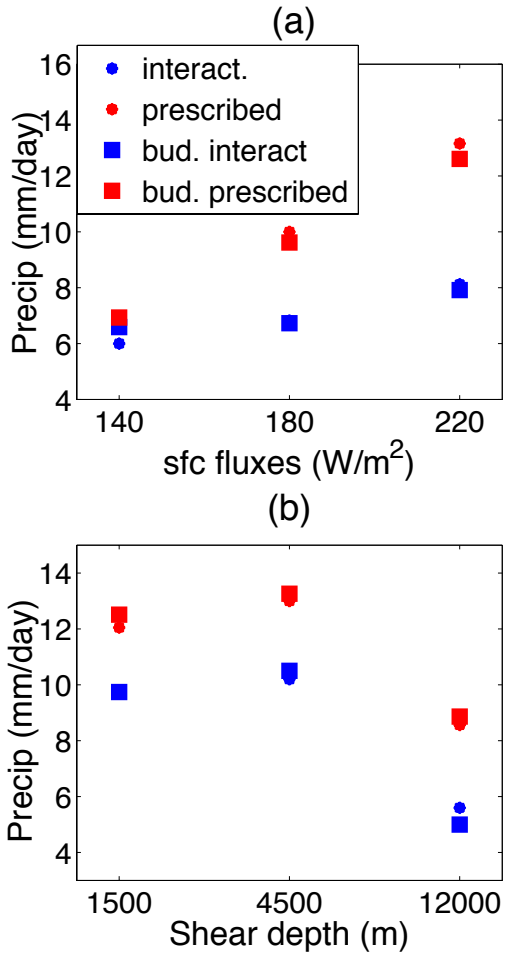

530

531 FIG.3. Domain averaged surface precipitation as a function of (a) surface fluxes in
532 unsheared environment, and (b) vertical wind shear depths at surface fluxes of 180 W
533 m^{-2}, for simulations of interactive (blue), and prescribed (red) radiation, stars denote
534 precipitation from model output, and squares denote precipitation diagnosed from the
535 moist and dry static energy budgets.
536

537

538

539

540

541

542

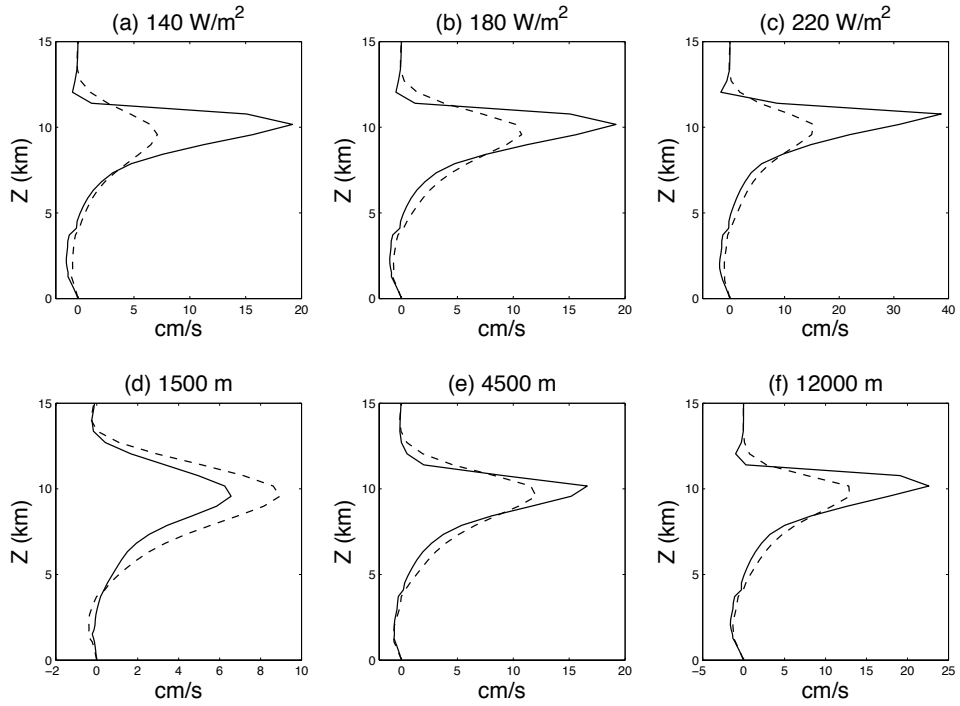

543

544

545 FIG.4. Domain averaged large scale vertical velocity W_{WTG} for different surface fluxes
546 (a)-(c) in unsheared environment, and different shear depths (d)-(f) at surface fluxes of
547 180 W m^{-2}, for simulation of interactive (continuous) and prescribed non-interactive
548 (dashed) radiative profiles.
549
550
551
552
553
554
555
556
557
558
559
560
561
562
563
564
565
566
567
568

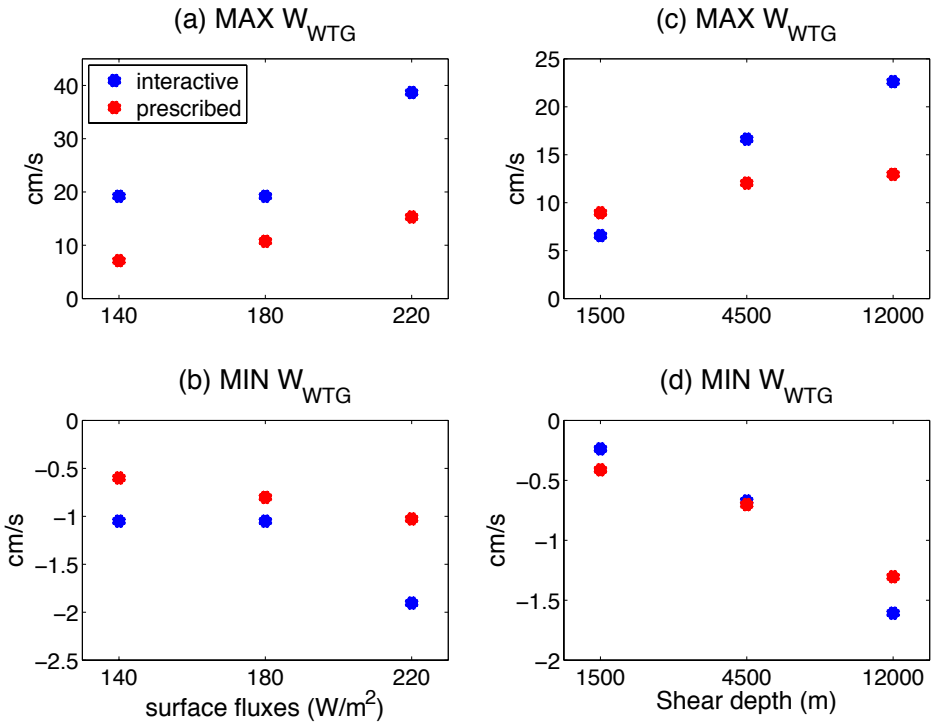

FIG.5. Large scale velocity of maximum (a),(c) ascending motion in the upper troposphere, and (b),(d) descending motion in the lower troposphere. (a) and (b) are cases of different surface fluxes in unsheared environment, and (c) and (d) for different shear depths at surface fluxes of 180 W m^{-2}. Simulations of interactive and prescribed non-interactive radiation are in blue and red, respectively.

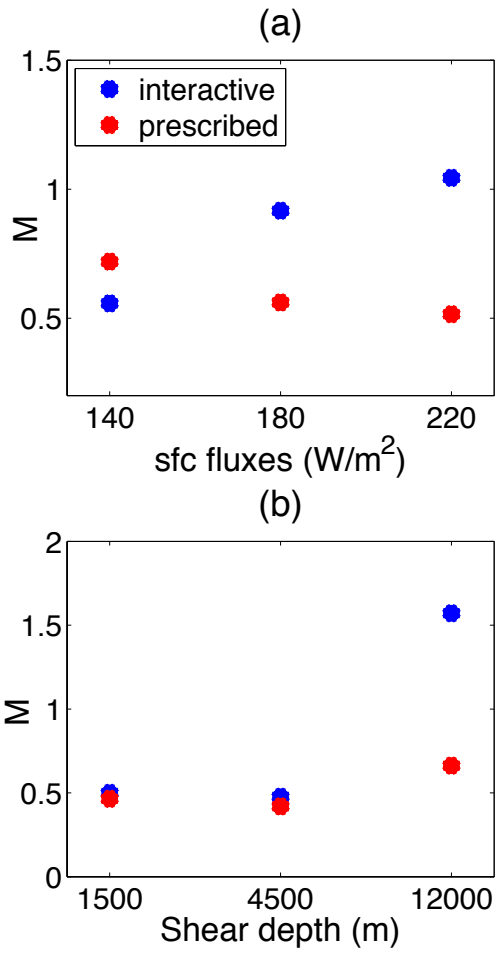

FIG.6. Normalized gross moist stability as a function of (a) surface fluxes in unsheared environment, and (b) vertical wind shear depths at surface fluxes of 180 W m^{-2}, for simulations of interactive (blue), and prescribed, non-interactive (red) radiation.

612

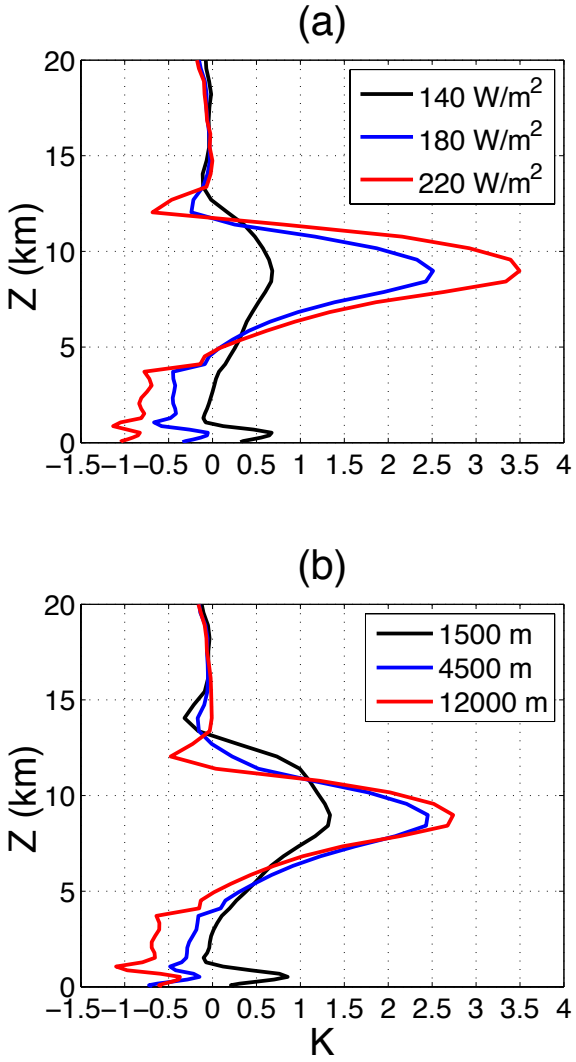

613
614 FIG.7. Domain mean profile of temperature anomalies, as departure from RCE profile, as
615 a function of (a) surface fluxes in unsheared environment, and (b) vertical shear depths at
616 surface fluxes of 180 W m^{-2}.
617
618